Bull. Mater. Sci. _####################_
https://doi.org/10.1007/s12034-022-02708-2

Boron-modified TiO_2 thin films for visible-light-driven photocatalysis

DORA ALICIA SOLIS-CASADOS[1,*], ESTEFANY RODRÍGUEZ-NAVA[2], RAFAEL BASURTO[3], UVALDO HERNÁNDEZ-BALDERAS[4], TATIANA KLIMOVA[5] and LUIS ESCOBAR-ALARCÓN[6]

[1]Universidad Autónoma del Estado de México, Centro Conjunto de Investigación en Química Sustentable UAEM-UNAM, C.P. 50200 Toluca, Mexico, Mexico

[2]Posgrado en Ciencia de Materiales, Universidad Autónoma del Estado de México, 50200 Toluca Estado de, Mexico, Mexico

[3]Departamento de Química, Instituto Nacional de Investigaciones Nucleares, Carr. México-Toluca S/N, C.P. 52750 La Marquesa Ocoyoacac, Mexico

[4]Instituto de Química, UNAM, CCIQS UAEM-UNAM, C.P. 04360 Mexico, Mexico

[5]Facultad de Química, Departamento de Ingeniería Química, UNAM, C.P. 04510 Mexico, Mexico

[6]Departamento de Física, Instituto Nacional de Investigaciones Nucleares, Carr. México-Toluca S/N, C.P. 52750 La Marquesa Ocoyoacac, Mexico

*Author for correspondence (solis_casados@yahoo.com.mx)

MS received 28 October 2021; accepted 6 March 2022

Abstract. Boron-modified TiO_2 thin films with different boron contents were obtained by the spin coating technique. Chemical composition and bonding were determined by X-ray photoelectron spectroscopy (XPS). Raman, UV–visible and photoluminescence spectroscopies were used to characterize the deposited films. XPS results revealed that the boron content varied from 2.1 to 9.0 at% and that Ti-O-B bonds are formed at the highest content. Raman spectra showed that incorporation of B in the titania lattice improved the crystallinity of the anatase phase and promoted a decrease in the crystallite size. Photoluminescence characterization indicated a quenching of the electron–hole recombination rate due to boron incorporation. The photocatalytic activity improved with films modified with B under solar-simulated irradiation.

Keywords. TiO_2 thin films; Boron; XPS; MG degradation; simulated solar light.

1. Introduction

Nowadays wastewater remediation is considered a key issue to provide clean water for human consumption and activities [1]. Water pollution originating from different anthropogenic activities is a topic that has been gaining importance in recent years because of its potential damage to the environment. To address this issue, several procedures have been proposed for wastewater treatment, such as absorption, biodegradation, chlorination and most recently the so-called advanced oxidation processes [2,3]. In general, terms, the advanced oxidation processes takes advantage of the high reactivity of OH radicals in oxidation processes that have proven their effectiveness for achieving the complete mineralization of organic pollutants [4,5]. Among the advanced oxidation processes, the photocatalysis process has proven to be a suitable green option for the treatment of wastewaters polluted with organic molecules. TiO_2 (titania) is considered the most popular photocatalyst owing to its physicochemical properties [6]. However, TiO_2 has two major drawbacks when used as a photocatalyst, its bandgap energy close to 3.2 eV, which makes it active only under UV light, and the higher recombination rate of photogenerated charges that it presents. Therefore, different strategies to overcome these disadvantages have been proposed, such as modifying the TiO_2 by doping with other elements or coupling it with other semiconductors. In this way it is possibly to reduce the bandgap energy to make TiO_2 photoactive under visible light as well as to decrease the recombination rate of the electron–hole pairs, both responsible for the good performance of the photocatalysts [6]. It is worth mentioning that our research group has investigated the modification of TiO_2 with metals such as Ni, Co, Fe, Ag, Au, Pt, Sn, Bi, non-metals such as N, and with a lanthanide Eu [7–13]. These studies have provided information about the effect of the modifiers on the physicochemical properties of TiO_2 as well as on the photocatalytic performance under solar light for the photodegradation of dyes as model molecules of pollutants contained in wastewaters. Another important aspect of our work is the use of photocatalysts in thin film form with some advantages over photocatalysts in powder form, as

nanoparticles or nanostructures in colloidal suspension, avoiding the difficulty of removing them from the reaction system [14,15], as well as the use of amounts of photocatalysts as low as 25 μg cm^{-2} [14]. In this work, we report the modification of TiO_2 with boron in thin film form with the purpose to obtain a visible-light-driven photocatalyst for the photodegradation of malachite green dye using a solar light simulated source.

2. Materials and methods

2.1 *Synthesis of thin films*

Thin films were deposited by the spin coating method spreading the precursor solutions, prepared by the sol–gel technique, at 3500 rpm onto glass substrates using a spin coater KW-4A from Chemat Technology. After deposition, the thin films were subjected to a thermal treatment at 400°C in a conventional oven at a heating rate of 3°C min^{-1} for 2 h.

Titanium isopropoxide ($Ti[OCH(CH_3)_2]_4$, Aldrich 97%), nitric acid (HNO_3, Fermont 70%), 2-propanol (CH_3-$CHOHCH_3$, Fermont 99.8%) and boric acid (H_3BO_3, Fermont) were the reagents used to prepare the precursor solutions. The synthesis was carried out under environmental conditions, mixing 5 ml of 2-propanol with 0.75 ml of titanium isopropoxide under continuous stirring. Subsequently, different quantities of boric acid (as a boron precursor) were added under stirring for 5 min to obtain theoretically 3, 5, 10 and 20 wt% of B_2O_3 in the titania film. The obtained films were labelled respectively as TiB1, TiB2, TiB3 and TiB4. The TiB0 sample containing only TiO_2 was used as reference. Afterwards, 1 ml of nitric acid was added to promote the transition of the sol to a gel-like. This procedure has been reported elsewhere for the preparation of TiO_2 thin films modified with different metals [7,12–14].

2.2 *Characterization of thin films*

The thin films were characterized by X-ray photoelectron spectroscopy (XPS) to determine the elemental chemical composition and the chemical bonding of the present

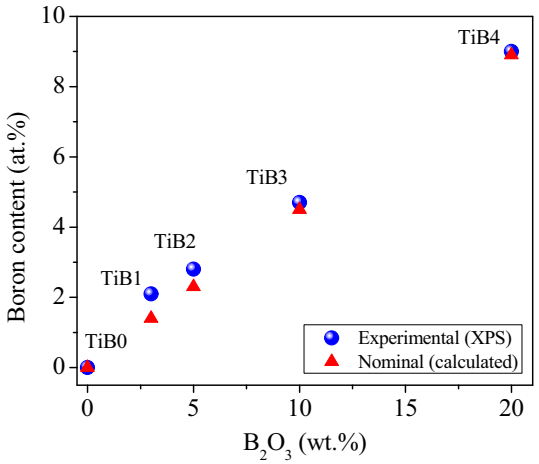

Figure 1. Boron content (nominal and experimental) as a function of the amount of B_2O_3 used in the synthesis.

elements. The XPS spectra were acquired from 50 to 1000 eV of binding energy in the high-resolution mode in the region of each element using a K-Alpha Thermo Scientific XPS spectrometer. The adventitious carbon peak was adjusted at 285 eV to correct any displacement due to sample charging. The microstructure of the thin films was characterized by Raman spectroscopy; spectra were recorded using a micro-Raman LabRam 800 system equipped with a confocal microscope Olympus BX40, samples were excited using a Nd:YAG laser (532 nm) at power levels close to 0.7 mW. The bandgap energy was calculated using the Tauc method from the transmittance spectra acquired from 200 to 1100 nm using a Perkin Elmer Lambda 35 UV-Vis spectrophotometer. Photoluminescence (PL) properties of the thin films were studied through PL spectroscopy using a spectrofluorometer FluoroMax 4 from Horiba Jobyn Ivon equipped with a 150 W Xenon lamp as an excitation source. Scanning electron microscopy (SEM) was used to observe the surface morphology of the thin films with a JEOL JSM-5900-LV microscope.

2.3 *Photocatalytic evaluation*

The photocatalytic performance of the obtained thin films was evaluated following the degradation of the malachite green (MG) dye. The degradation reaction was performed in

Table 1. Elemental chemical composition obtained from XPS.

Photocatalyst	Ti (at%)	O (at%)	B (at%) experimental	B (at%) nominal	B_2O_3 (wt%)
TiB0	32.0	68.0	0	0	0
TiB1	30.6	67.3	2.1	1.4	3
TiB2	37.0	60.2	2.8	2.3	5
TiB3	27.2	68.1	4.7	4.5	10
TiB4	31.0	60.0	9.0	8.9	20

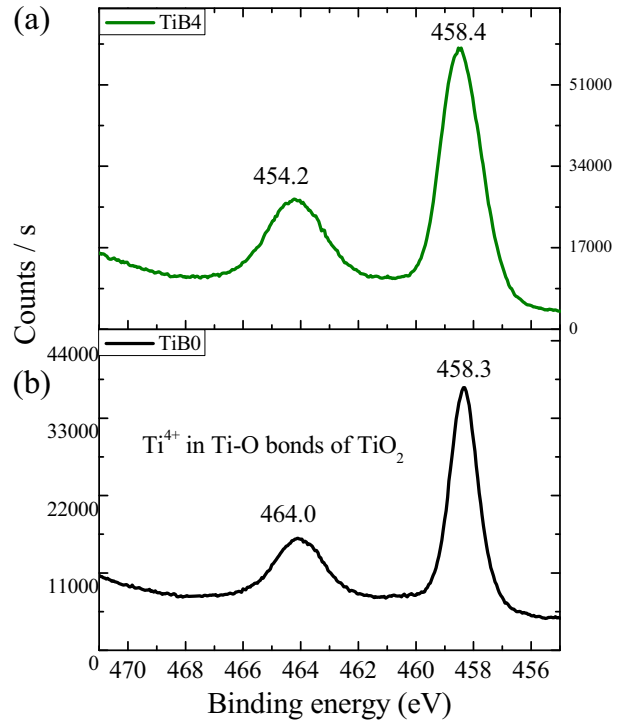

Figure 2. XPS Ti-2p region corresponding to films (**a**) without boron (TiB0) and (**b**) containing 9.0 at% of boron (TiB4).

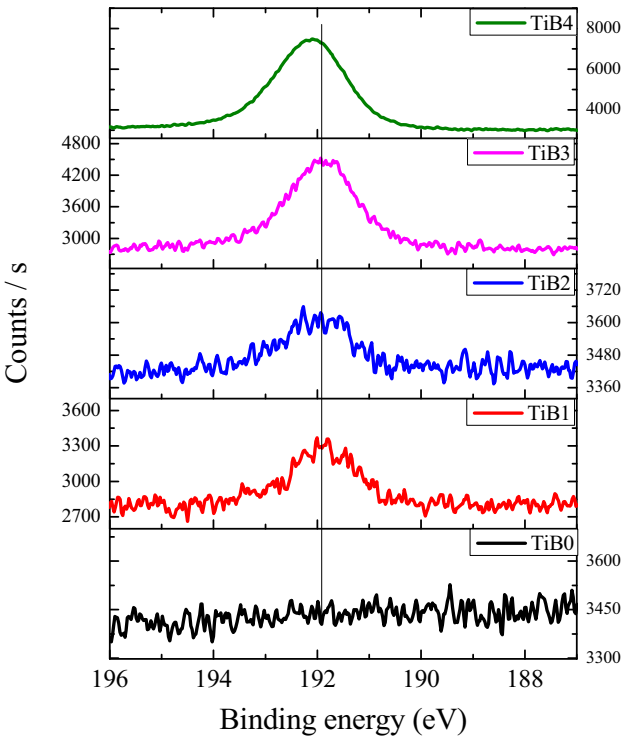

Figure 3. XPS B-1S region of films with different boron contents: 0, 2.1 at%, 2.8 at%, 4.7 at% and 9.0 at%.

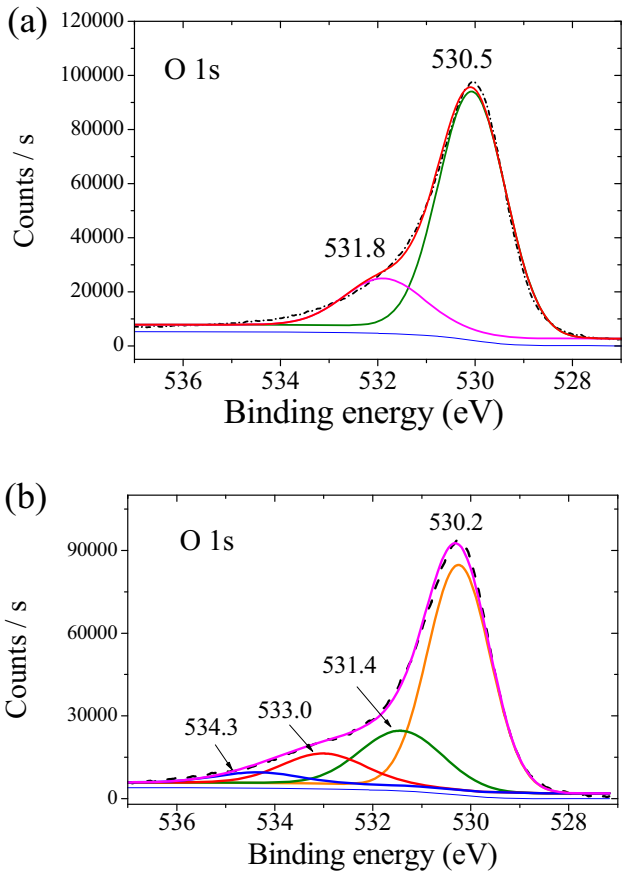

Figure 4. XPS O-1s region corresponding to films (**a**) without boron and (**b**) containing 9.0 at% of boron.

a batch reactor where a piece of 1 cm^2 of the photocatalyst thin film (approximately 25 μg of mass, lower than that used in powder form) was introduced into 25 ml of an aqueous solution of the MG dye (10 μmol l^{-1}). Initially, the reaction was evaluated in dark conditions in the uncatalysed and catalysed process, where reaction and absorption onto the thin films was dismissed. Afterwards, the photocatalytic reaction was carried out by stirring for 15 min in dark conditions to reach the equilibrium between the thin film used as a photocatalyst and the dye solution to discard the absorption process. Photocatalytic reaction was activated by illuminating the thin films with light emitted by a solar simulator (Sciencetech SF150 model, class A) at an average intensity close to 60 mW cm^{-2}. The degradation degree of the MG dye was followed by the decrease of its characteristic absorption band peaking at 617 nm, this was carried out by taking aliquots each 15 min for the 2 h of reaction time. Previously, a calibration curve of absorbance of the MG dye as a function of the concentration was traced. Kinetic rate constants were obtained, considering a first-

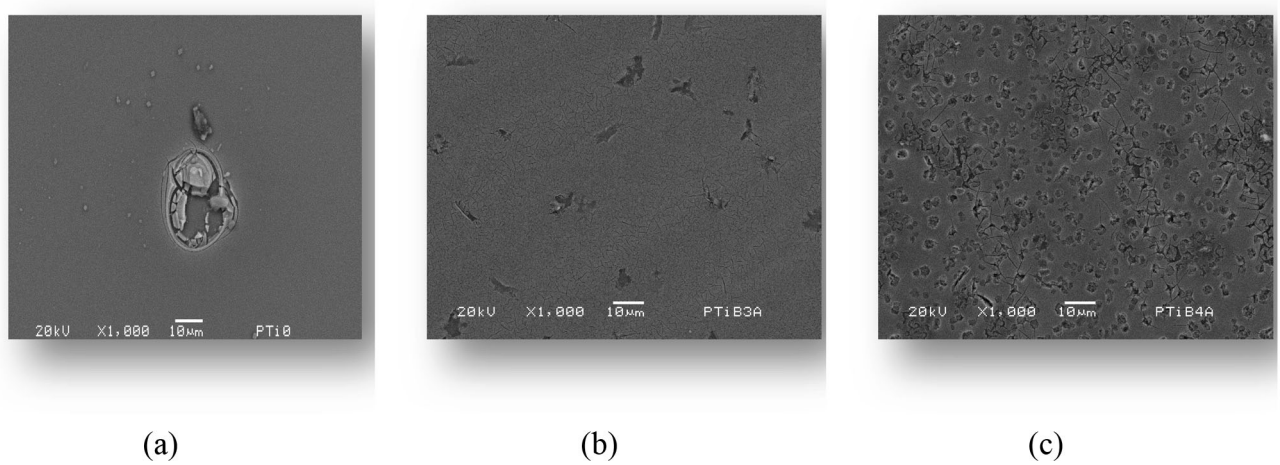

Figure 5. Surface morphology of films: (**a**) without boron, (**b**) 4.7 at% of B and (**c**) 9.0 at% of B.

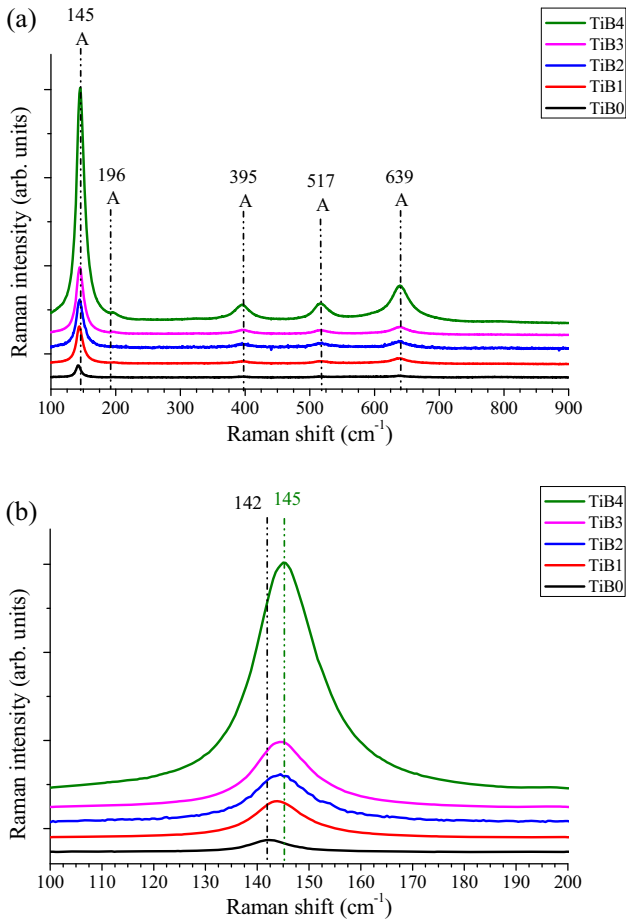

Figure 6. (**a**) Raman spectra of the B-modified TiO_2 thin films, (**b**) zoom of the 144 cm^{-1} Raman band.

order kinetic model, from the slope of the plot of natural logarithm of MG concentration *vs.* reaction time.

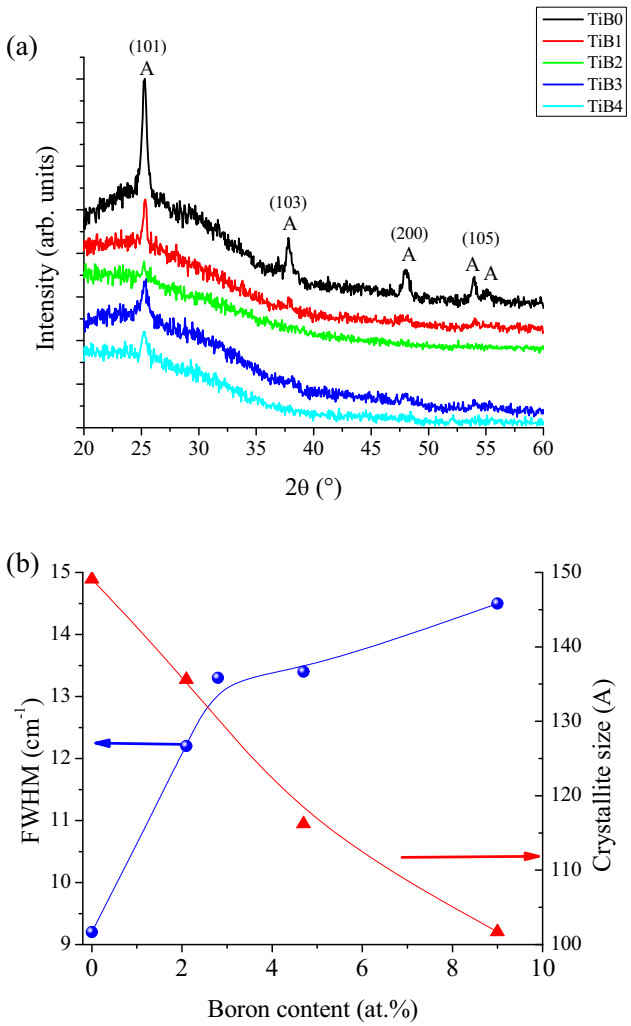

Figure 7. (**a**) XRD patterns of the B-modified TiO_2 thin films, (**b**) full-width at half-maximum of the Raman peak at 145 cm^{-1} and crystallite size as a function of the boron content.

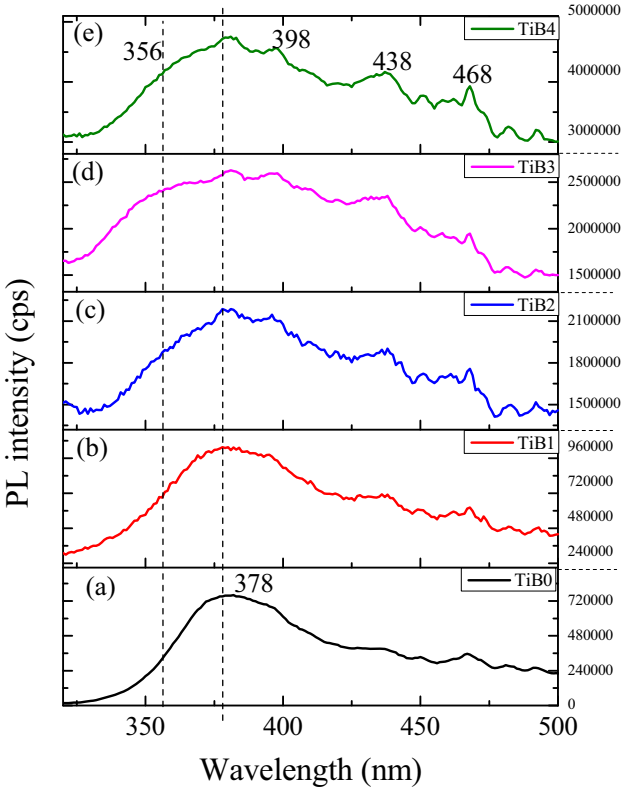

Figure 8. PL spectra of the different photocatalysts.

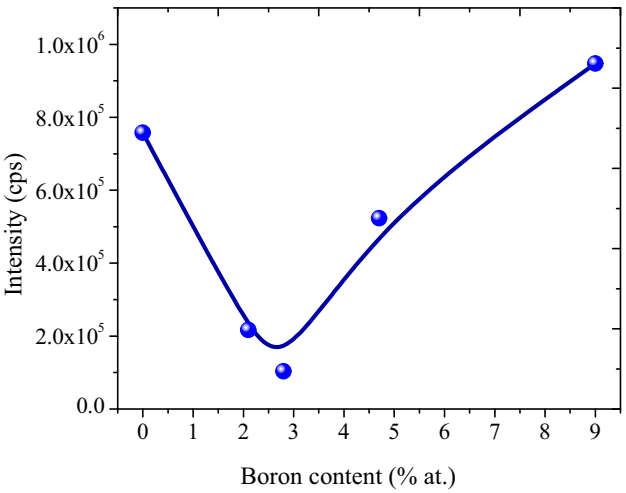

Figure 9. PL intensity *vs.* boron content.

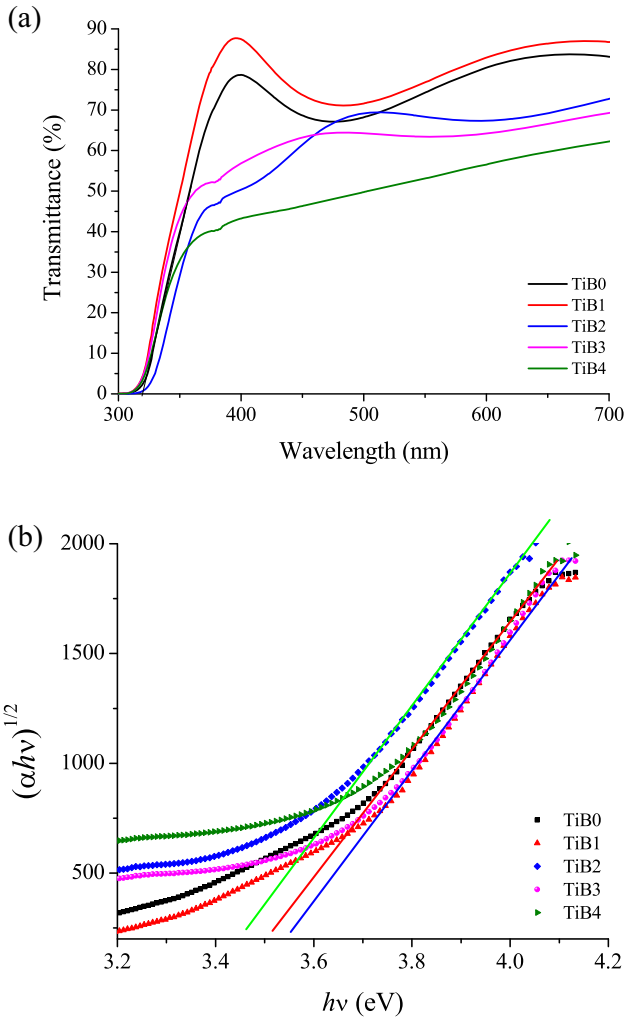

Figure 10. (**a**) Transmittance spectra and (**b**) Tauc plots corresponding to different thin films.

Table 2. Optical bandgap energy of the TiB thin films.

Photocatalyst	Boron content (at%)	E_g (eV)
TiB0	0.0	3.0
TiB1	2.1	3.1
TiB2	2.8	3.1
TiB3	4.7	3.3
TiB4	9.0	3.4

3. Results

3.1 *Characterization of thin films*

Table 1 shows the chemical composition determined from the XPS spectra (experimental) and calculated as the expected load of B_2O_3 (nominal) to obtain theoretically 3, 5, 10 and 20 wt% as B_2O_3 in the titania film. In general terms, it can be seen that the boron content in the films varies from 2.1 to 9.0 at%. These data are plotted in figure 1, in which a good correlation between both values, the nominal and the experimental, of boron content with the amount of B_2O_3 used for the synthesis is observed. The linear behaviour observed suggests that the proposed procedure enables controlling the B content in the thin films in an easy way.

High-resolution XPS measurements were performed for all samples to determine the chemical bonding of the

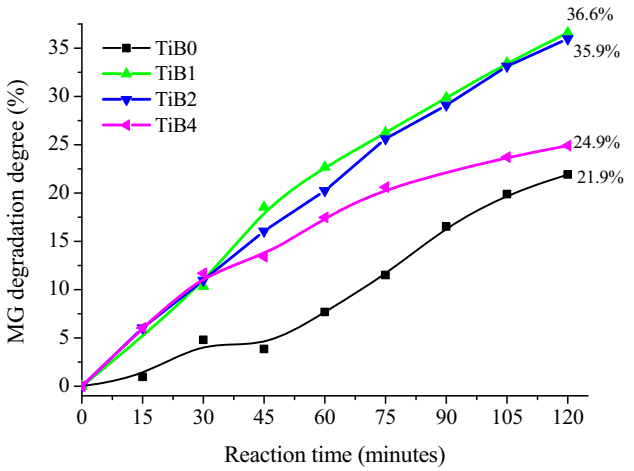

Figure 11. Malachite green dye degradation as a function of the reaction time for the prepared photocatalysts.

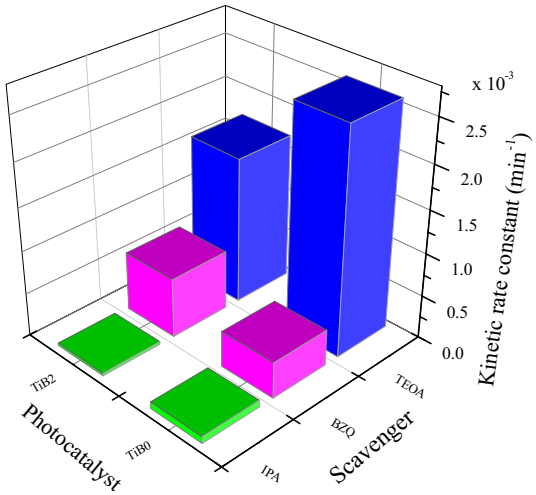

Figure 12. The kinetic rate constants of the MG degradation reactions using scavengers.

Table 3. Kinetic rate constants obtained assuming a first-order reaction.

Photocatalyst	Boron content (at%)	Kinetic rate constant under simulated solar light ($\times 10^{-3}$, min^{-1})
TiB0	0.0	2.0
TiB1	2.1	3.2
TiB2	2.8	3.9
TiB3	4.7	*
TiB4	9.0	2.6

*Not possible to calculate.

present elements Ti, O and B. Figure 2 shows the XPS Ti2p region spectra of the sample TiB0, without boron (figure 2a) and of the sample TiB4, with the highest boron content (figure 2b). In both cases, a doublet with peaks close to 464.0 and 458.3 eV is observed. These binding energies agree well with Ti-O bonds in TiO_2 [16]. Spectrum of the film containing 9.0 at% of boron shows broader signals than the spectrum of the film without B, indicating a variation of the chemical bonding environment of Ti due to the boron incorporation. Figure 3 shows the XPS B1s region spectra of the prepared films with different content of boron. The spectra of samples TiB1, TiB2 and TiB3 show a peak at 191.9 eV, whereas the peak for the sample TiB4 is slightly shifted to 192.1 eV suggesting the formation of B_2O_3. Figure 4 shows the O1s region spectra of the sample without boron (figure 4a) and of the sample containing 9.0 at% of boron (figure 4b). These spectra show asymmetric peaks with tails extending to high binding energies. These peaks were fitted using Voigt line shapes, which are shown in these figures. The most intense peak around 530.2 eV is attributed to O-Ti bonds, indicating the presence of TiO_2 [17]. The peak close to 531.4 eV is attributed to O-H bindings and is due to adsorbed moisture from the atmosphere [17]. Two additional signals appear in the sample with boron, the first one at 533.0 eV is attributed to B-O bonds confirming the presence of Ti-O-B bonds, whereas the peak at 534.3 eV is due to adsorbed water also due to adsorbed moisture from the atmosphere [18].

Surface morphology observed from SEM images show reasonably smooth surfaces with some defects that increase in number as the boron content increases, as is seen in figures 5a–c. It is worth noting that these changes in morphology due to B incorporation could be useful for photocatalytic applications, because the specific surface area increases as a function of the boron content.

The Raman spectra shown in figure 6a display the characteristic vibrational modes of the anatase crystalline phase of TiO_2 at 145 cm^{-1} (E_g), 196 cm^{-1} (E_g), 395 cm^{-1} (B_{1g}), 517 cm^{-1} ($A_{1g} + B_{1g}$) and 639 cm^{-1} (E_g) [19]. Two main changes in the Raman spectra due to boron incorporation are observed. The first one is a monotonic increase in the Raman intensity of the peak at 145 cm^{-1} as a function of the boron content, suggesting that boron promotes a better degree of crystallinity of the anatase phase as the B content increases. The second one is a slight shift of the main vibration mode from 142 to 145 cm^{-1} as the boron content increases as is shown in the zoom of the vibrational mode at 142 cm^{-1} (E_g) in figure 6b.

Figure 7a shows the XRD patterns of the prepared films with different boron content. Crystalline phase identification was done by comparison using the powder diffraction file (PDF) data bank supplied by the International Centre for Diffraction Data (ICDD). The spectrum of the sample without boron shows clear diffraction lines at 25.30, 37.85, 48.20, 53.95 and 55.10°, characteristics of the anatase phase of TiO_2 (00-021-1272).

The average crystallite size was estimated by using the Debye-Scherrer equation:

$$D = \frac{k\lambda}{\beta\cos\theta},$$

where D is the mean crystallite size, λ the wavelength of the radiation (1.540598 Å for Cu-Kα radiation), k a dimensionless number of the order of unity, known as the Scherrer constant whose value depends on the shape of the crystal, the size distribution and how the width is determined, β the peak full-width at half-maximum intensity and θ is the peak position in radians [20]. The results show that the average crystallite size decrease with the increment of B content, the values varied from 14.9 to 10.2 nm for the TiO_2 and the film with a boron content of 9.0 at%, respectively.

Figure 7b shows the full-width at half-maximum of the Raman peak at 145 cm^{-1} as a function of the boron content. The same graph shows the crystallite size determined from the XRD patterns. An increased broadening with the boron content and at the same time a decrease of the crystallite size are observed, which is in good agreement with previous reports [21].

The PL spectrum of the TiO_2 film (figure 8a) exhibits a band emission peaking at 378 nm that can be attributed to an interband transition in good agreement with the bandgap value of titania (3.2 eV). When boron is incorporated in the films, the spectra show changes in the PL emission, becoming broader with the increase in boron content and displaying signals at 398, 438 and 468 nm that are clearly seen in the spectrum of figure 8e. The last two signals can be attributed to free and bounded excitons, respectively [22]. Another change is the appearance of a shoulder peaking at 356 nm, indicating a widening of the bandgap. Figure 9 displays the PL intensity as a function of the boron load, which shows that boron incorporation at lower loads produces a strong quenching of the PL emission, indicating a decrease of the recombination rate due to the boron presence.

The optical bandgap energy was estimated from the transmittance spectra, shown in figure 10a, using the Tauc method by plotting $(\alpha h\nu)^{1/2}$ as a function of the photon energy ($h\nu$). The optical absorption coefficient was obtained using the equation:

$$\alpha = -\ln(T)/t,$$

where T is the transmittance and t the thickness of the film. The E_g values were then calculated by a linear fit of the linear part of the curve, determining its intersection with the photon energy axis as the quotient of the intercept to the slope [23,24]. Figure 10b shows the Tauc plots and three of the lineal fittings performed. The obtained E_g values are shown in table 2 and indicate an increase from 3.03 to 3.38 eV as the B content increases.

3.2 *Photocatalytic evaluation of thin films*

Figure 11 shows the degradation degree of MG dye achieved with the different samples. The TiO_2 thin film without boron reached 21.9% of degradation, the lowest value. The photocatalytic response of the samples with the lower content of boron, 2.1 and 2.8 at%, follows a very similar behaviour, reaching conversions of 36.6 and 35.9%, respectively. Further increase in the boron content to 9.0 at% decreases the degradation degree to 24.9%. The kinetic rate constants shown in table 3 were calculated assuming a first-order kinetic reaction as the slope from the plot of the natural logarithm of MG concentration *vs.* reaction time. The highest kinetic rate constant corresponds to the TiB2 photocatalysts, followed by the TiB1 film.

In order to gain insight about the chemistry, radicals involved, and the reaction routes in the degradation process of the MG dye by photocatalysis, scavenger molecules were used. The p-Benzoquinone (BZQ, 0.001 M) molecule was used to trap the superoxide radicals (O_2•); triethanolamine (TEOA, 0.01 M) was used to block holes (h^+) and 2-propanol (IPA, 0.02 M) was added to trap the hydroxyl radicals (OH•) [25–28]. Two photocatalysts were used in the degradation reactions under the previous conditions by adding these scavenger molecules separately to the reaction systems, using the TiO_2 thin film and using the TiO_2 film modified with 2.8 at% of boron; this sample was chosen because it gave the highest MG degradation. Figure 12 summarizes the results showing the kinetic rate constants determined in each case. In the first case, the results show that the kinetic rate constants are in the following order IPA $<$ BZQ $<$ TEOA. This indicates that holes (h^+) and OH• radicals have a lower contribution to the dye degradation. The incorporation of IPA to the reaction system results in the lowest kinetic rate constant, suggesting that the OH• radicals have an important contribution to the MG degradation. When TEOA is used, the highest kinetic rate constant is reached. This result, together with the previous one, reveal that the preferred route for degradation of the malachite green dye is the reduction path with the superoxide radicals being responsible of the MG degradation. When boron is used to modify the TiO_2, the results are different. In this case, the use of BZQ results in a kinetic rate constant higher than in the previous case, suggesting a major contribution of the h^+ and OH• radicals to the photocatalytic degradation of MG. Incorporation of IPA to the reaction system results in the lowest kinetic rate constant value, which proves that the OH• is the radical with the major contribution to the MG degradation. Finally, the use of TEOA in the reaction system favors the availability of superoxide radicals for the degradation reaction.

4. Discussion

XPS spectrum of the B1s region suggests that boron is at interstitial positions in the titania lattice, because the B-O binding energy in B_2O_3 is at 193 eV and the B-Ti binding energy is at 187.5 eV, and therefore the observed signal could be attributed to Ti-O-B bonds [18]. The slight binding

energy shift observed for the sample with the highest boron load (figure 3e) could be due to an increase in the number of B-O bonds starting the formation of B_2O_3. The incorporation of B in the titania lattice is also inferred from the Raman shift of the peak at 142 cm^{-1} that can be due to compressive stress induced by B incorporation as well as due to the improved crystallinity of anatase, also promoted by B. The bandgap values obtained for the samples with the lower B content and without B are consistent with the bandgap value of the anatase phase of TiO_2. Also, this increase in the bandgap can be related to the decrease of the crystallite size found by Raman spectroscopy and XRD.

Concerning PL results, for photocatalytic applications a key issue is to investigate the recombination rate of photogenerated electron–hole pairs since they are responsible for the formation of the reactive species that degrade organic molecules. The obtained results show that boron incorporation at lower loads produces a strong quenching of the PL emission, whereas at the highest boron content the PL intensity becomes even higher than the emission of the titania film. It has been reported that the lower the PL intensity, the lower the recombination rate of photo-induced electron–hole pairs, and the higher the photocatalytic activity of semiconductor photocatalysts [29]; therefore, it is expected that samples TiB1 and TiB2 show better photocatalytic activity which is observed in the photocatalytic results. It is important to emphasize that thin films containing boron present better photocatalytic activity than the thin film without boron. It is also important to remark that boron-modified TiO_2 photocatalysts can be considered visible-light-driven photocatalysts, as they were tested under simulated solar light, achieving a photocatalytic activity 65% higher than the photocatalytic degradation reached with the TiO_2 thin film, which can be attributed to the decrease in the recombination rate of the electron–hole pairs. The obtained results of photocatalytic reactions using scavengers indicate that modification of TiO_2 with boron changes the degradation reaction routes increasing the participation of the OH• radicals, which could explain the improved photocatalytic response of the TiB2 sample observed in figure 11. Additionally, in both cases it is found that the preferred route for degradation of the malachite green dye is the reduction path driven by the O_2• radicals. The main finding to elucidate the preferential reaction route is that the reduction/oxidation ratio changes from 6.3 to 2.5 when boron is incorporated to the TiO_2 photocatalyst.

5. Conclusions

Boron-modified TiO_2 thin films with boron contents from 2.1 to 9.0 at% were successfully obtained by the spin coating technique. The proposed experimental procedure allows controlling the amount of boron incorporated in the thin film in an easy way. It was found that boron interacts with the TiO_2 lattice producing new bonds. At lower amounts of boron incorporated into the TiO_2 lattice, the electron–hole recombination decreases and consequently improves the degradation degree by around 65% for the best film, the film with 2.8 at% of boron, with respect to the film without boron. The prepared boron-modified TiO_2 thin films can be considered visible-light-driven photocatalysts because they were tested under simulated solar light. Additionally, it is worth mentioning that the achieved photocatalytic activity using thin films is reached using very low amounts of photocatalysts, typically of the order of tens to hundreds of μg. The use of scavengers reveals that the O_2• radicals are the reactive species responsible for the MG dye degradation.

Acknowledgments

We acknowledge SIEA-UAEM for financial support through the project 6537, the technical assistance of LIA Citlalit Martínez, Dr Diego Martínez-Otero, M en C. Nieves Zavala, M en C. Lizbeth Triana, M en C. Melina Tapia, M en C Alejandra Núñez.

References

[1] Nirupama and Mandal B K 2022 *Biointerface Res. Appl. Chem.* **12** 2535
[2] Chen D, Sivakumar M and Ray A K 2000 *Dev. Chem. Eng. Min. Process* **8** 505
[3] Zhu S and Wang D 2017 *Adv. Energy Mater.* **7** 1700841
[4] Sakthivel S, Neppolian B, Shankar M V, Palanichamy M and Murugesan V 2003 *Sol. Energy Mater. Sol. Cells* **77** 65
[5] Ibhadon A O and Fitzpatrick P 2013 *Catalyst* **3** 189
[6] Zangeneh H, Zinatizadeh A A L, Habibi M, Akia M and Hasnain Isa M 2015 *J. Ind. Eng. Chem.* **26** 1
[7] Solis-Casados D A, Escobar-Alarcón L, Fernández M and Valencia F 2013 *Fuel* **110** 17
[8] Pérez-Álvarez J, Solis-Casados D A, Romero S and Escobar-Alarcón L 2014 *Adv. Mater. Res.* **976** 212
[9] Escobar-Alarcón L, Velarde Granados E, Villa Sánchez D, Olea-Mejia O, Haro-Poniatowski E and Arrieta Castañeda A 2014 *Adv. Mater. Res.* **976** 196
[10] Escobar-Alarcón L, Solis-Casados D A, Romero S and Haro-Poniatowski E 2020 *Appl. Phys. A* **126** 57
[11] Solis-Casados D A, Escobar-Alarcón L, Gómez-Olivan L M, Haro-Poniatowski E and Klimova T 2017 *Fuel* **198** 3
[12] Solis-Casados D A, Escobar-Alarcón L, Alvarado Pérez V and Haro-Poniatowski E 2018 *Int. J. Photoenergy* **2018** 8715987
[13] Solis-Casados D, Martínez Peña J, Hernández-López S and Escobar-Alarcón L 2020 *Top. Catal.* **63** 564
[14] Escobar Alarcón L and Solis-Casados D A 2021 *MundoNano* **14** 10
[15] Pedanekar R S, Shaikh S K and Rajpure K Y 2020 *Curr. Appl. Phys.* **20** 931
[16] Jose A, Oliver B and Elisa R 2004 *Surf. Sci.* **549** 134

[17] McCaterty E and Wightman J P 1998 *Surf. Interface Anal.* **26** 549
[18] Jung Kyeong Youl, Park Seung Bin and Ihmb Son-Ki 2004 *Appl. Catal. B* **51** 239
[19] Balachandran U and Eror N G 1982 *J. Solid State Chem.* **42** 276
[20] Langford J I and Wilson A J C 1978 *J. Appl. Cryst.* **11** 102
[21] Maniua D, Iliescua T, Ardeleana I, Cinta-Pinzarua S, Tarceab N and Kiefer W 2003 *J. Mol. Struct.* **651** 485
[22] Haonan G, Feiyan X, Bei Ch, Jiaguo Y and Wingkei H 2019 *Chem. Cat. Chem.* **11** 6301
[23] Escobar-Alarcón L, Arrieta A, Camps E, Muhl S, Rodil S and Vigueras-Santiago E 2007 *Appl. Surf. Sci.* **254–1** 412
[24] Daimei Ch, Dong Y, Qun W and Jiang Zhongyi 2006 *Ind. Eng. Chem. Res.* **45** 4110
[25] Difa X, Bei Ch, Shaowen C and Jiaguo Y 2015 *Appl. Cat. B: Environm.* **164** 380
[26] Chien-Kai H, Tsunghsueh W, Chang-Wei H, Chi-Yung L, Mei-Yao W and Yang-Wei L 2017 *Appl. Surf. Sci.* **399** 10
[27] Lei X, Yongge W, Wan G, Yihang G and Yingna G 2015 *Appl. Surf. Sci* **332** 682
[28] Si-Zhan W, Kui L and Wei-De Z 2015 *Appl. Surf. Sci.* **324** 324
[29] Jing L, Qu Y, Wang B, Li S, Jiang B, Yang L *et al* 2006 *Sol. Energy Mater. Sol. Cells* **90** 1773